Carrier Transport in Polycrystalline Transparent Conductive Oxides: A Comparative Study of Zinc Oxide and Indium Oxide

Klaus Ellmer, Rainald Mientus*

Hahn-Meitner-Institut, Dept. Solar Energetics, Glienicker Str. 100, 14109 Berlin, Germany
Tel +49-30-80622770, Fax +49-30-80622434, E-Mail ellmer@hmi.de
* Opto-Transmitter-Umweltschutz-Technologie e.V., D-12555 Berlin, Köpenicker Str.325[b]
Germany, Tel +49-30-65762673, Fax +49-30-65762672, E-Mail r.mientus@t-online.de

Abstract

Highly-doped indium-tin oxide films exhibit resistivities ρ as low as $1.2 \cdot 10^{-4}$ Ωcm, while for ZnO films resistivities in the range of 2 to $4 \cdot 10^{-4}$ Ωcm are reported. This difference is unexpected, if ionized impurity scattering would be dominant for carrier concentrations above 10^{20} cm^{-3}. By comparing the dependences of the effective Hall mobility on the carrier concentration of ZnO and ITO it is found that grain barriers limit the carrier mobility in ZnO for carrier concentrations as high as $2 \cdot 10^{20}$ cm^{-3}, independently, if the films were grown on amorphous or single crystalline substrates. Depending on the deposition method, grain barrier trap densities between 10^{12} to $3 \cdot 10^{13}$ cm^{-2} were estimated for ZnO layers. Also, crystallographic defects seem to reduce the mobility for highly doped ZnO films. On the other hand, for ITO films such an influence of the grain barriers was not observed down to carrier concentrations of about 10^{18} cm^{-3}. Thus the grain barrier trap densities of ZnO and ITO are significantly different, which seems to be connected with the defect chemistry of the two oxides and especially with the piezoelectricity of zinc oxide.

Keywords Transparent conductive oxides, carrier transport, degenerate semiconductors, grain barriers, electron mobility

1. Introduction

Transparent conductive oxides constitute a material class that combines high transparency in the visible and near infrared spectral range with a high electrical conductivity of up to 10^3 to 10^4 Scm^{-1}.

Today, films of indium, zinc and tin oxide are widely used as transparent electrodes in flat panel displays, thin film solar cells, as heating or antistatic layers. Up to now, tin-doped indium oxide (ITO) yields the lowest resistivities of about $1 \cdot 10^{-4}$ Ωcm. This, together with its very good etchability, are the reasons why ITO is presently used exclusively as transparent electrode material for flat panel displays, based on liquid crystals, microplasmas or organic light emitting diodes (OLED). Zinc oxide, which is much less expensive than indium oxide, would be an alternative to replace ITO in flat panel displays. It can be doped by group III elements (boron, aluminium, gallium or indium) up to carrier concentrations of more than 10^{21} cm^{-3}. However, for ZnO only resistivities in the range of 2 to $4 \cdot 10^{-4}$ Ωcm have been reported, particularly when prepared by large area coating methods like magnetron sputtering. Furthermore, compared to ITO it is much more difficult to prepare doped ZnO films of such low resistivities, i.e. the "process window" is much narrower.

It has been stated by Bellingham et al. and others [1-3] that the carrier scattering at ionized impurities (for instance Sn^+ or Al^+) limits the mobility in these TCO materials for carrier concentrations above 10^{19} cm^{-3}. For a degenerately doped semiconductor the mobility due to ionized impurities μ_{ii} is proportional to the square of the ratio of its relative dielectricity constant and its effective mass [4-6]: $\mu_{ii} \sim (\varepsilon_r/m^*)^2$. This ratio is listed in Table 1 for the three oxides. The data of silicon are included for comparison, since this semiconductor is best investigated for carrier concentrations $>10^{19}$ cm^{-3}.

Table 1: Static dielectric constants ε_r, effective masses m^*/m_e and ionized-impurity limited mobilities of TCOs and of silicon

Material	ε_r	m^*/m_e	$(\varepsilon_r\, m_e/m^*)^2$	Normalized Ratio	μ_{ii} [cm^2/Vs]
In_2O_3	9	0.35	661	0.53	50
SnO_2	11.5	0.26	1956	1.57	30
ZnO	8.3	0.28	879	0.70	50
Si	11.9	0.337	1247	1.0	68.5(n)/44.5(p)

If ionized impurity scattering would be the dominant scattering mechanism for carrier densities > 10^{19} cm^{-3}, comparable resistivities for ITO and ZnO are expected for the same carrier concentrations. For SnO_2 even higher mobilities can be calculated, about a factor of 2 to 3 higher than that of ZnO or ITO. However, this is not found experimentally [2].
Therefore, in the present study the carrier transport processes in ITO and ZnO are compared in order to get a deeper understanding of the differences between these TCO materials. For this purpose conductivity and Hall mobility measurements on ZnO:Al and ITO films were undertaken for films deposited on amorphous as well as single crystalline substrates (sapphire) in order to determine the dominant scattering processes (ionized impurities, grain barriers, crystallographic defects). Our own data are compared with literature data reported for ZnO and ITO to show the general trends. Theoretical and semiempirical models are used to fit the experimental data and to derive characteristic material parameters for these three oxides.

2. Theoretical models

The theoretical models on ionized impurity scattering were already reviewed in 2001 by one of the authors when estimating the mobility limit of highly-doped zinc oxide [3]. In the following a short summary is given to lay the basis for the further discussion.
Ionized impurity scattering. This scattering process is caused by ionized dopant atoms and dominates for carrier concentrations above about 10^{19} cm^{-3}. An analytical expression for the mobility μ_{ii} of degenerately doped semiconductors, taking into account the non-parabolicity of the conduction band, was given by Zawadzki [7] and refined by Pisarkiewicz et al. [6]:

$$\mu_{ii}^{ZP} = \frac{3(\varepsilon_r\varepsilon_0)^2 h^3}{Z^2 m^{*2} e^3} \frac{n}{N_i} \frac{1}{F_{ii}^{np}(\xi_d)} \quad \text{with} \quad \xi_d = \left(3\pi^2\right)^{1/3} \frac{\varepsilon_r\varepsilon_0 h^2 n^{1/3}}{m^* e^2} \qquad (1),$$

where the screening function F_{ii}^{np} is given by

$$F_{ii}^{np} = \left[1 + \frac{4\xi_{np}}{\xi_d}\left(1 - \frac{\xi_{np}}{8}\right)\right] \cdot \ln(1+\xi_d) - \frac{\xi_d}{1+\xi_d} - 2\xi_{np}\left(1 - \frac{5\xi_{np}}{16}\right) \qquad (2),$$

with the parameter ξ_{np}=1-m_0*/m*, which describes the non-parabolicity of the conduction band (m*, m_0* - effective masses in the conduction band and at the conduction band edge,

respectively). The prefactor in equ.(1) shows, that the ionized-impurity limited mobility depends as $\mu_{ii} \sim (\varepsilon_r/m^*)^2$ on the material constants of the semiconductor and as $\mu_{ii} \sim Z^{-2}$ on the charge of the dopants.

The theoretical model given above as well as the models of Conwell and Weisskopf [8,9], Shockley [4], and Dingle [5] are based on the assumption of a statistically homogeneous distribution of scattering centers, i.e. dopants. However, this is no longer valid for extremely high dopant concentrations, where the dopants form clusters which lead, due to their higher charge ($\mu_{ii} \sim Z^{-2}$), to lower mobilities. This effect was already proposed in 1971 by Dakhovskii et al. [10]. Klaassen applied this cluster model to fit accurate measurements of mobilities in p- and n-type single crystalline silicon [11,12]. He calculated cluster charges up to 2 for boron-doped and 3.5 for phosphorous-doped silicon at a carrier concentration of 10^{21} cm^{-3}. Recently, such clusters of zinc dopants were verified by atomically-resolved analysis in GaAs [13]. The carrier mobility in highly-doped semiconductors is best investigated for p- and n-type silicon. Masetti et al. [14] measured the mobility of arsenic-, phosphorus-, and boron-doped silicon up to carrier concentrations of $5 \cdot 10^{21}$ cm^{-3} and fitted their experimental values by the empirical curve

$$\mu^{Ma} = \mu_{min} + \frac{\mu_{max} - \mu_{min}}{1 + \left(n / n_{ref1}\right)^{\alpha_1}} - \frac{\mu_1}{1 + \left(n_{ref2} / n\right)^{\alpha_2}} \qquad (3).$$

The fit parameters μ_{max}, μ_{min} and $\mu_{min} - \mu_1$ describe the lattice mobility at low carrier concentrations, the mobility limited by ionized impurity scattering and the clustering mobility, discussed above (see Table 2).

Unfortunately, experimental mobility data for single crystalline oxides are not available for $N > 10^{20}$ cm^{-3}. For zinc oxide mobilities up to $N \approx 8 \cdot 10^{19}$ cm^{-3} have been measured by Rupprecht about 50 years ago [15]. His data are shown in Fig.1 together with other data for single crystalline ZnO as well as the fit curves for the experimental data of silicon given by Masetti et al. [14]. The ZnO mobility values were fitted using the empirical formula (3) and the fit parameters are summarized in Table 2 together with the corresponding values for silicon. In the transition region from lattice to ionized scattering for $5 \cdot 10^{16} < N < 5 \cdot 10^{18}$ cm^{-3} a large scattering of the experimental ZnO data can be observed. Therefore, the data have been fitted in analogy to the silicon data, which exhibit a much higher accuracy [14]. However, the exact transition does not influence the conclusions much since we are interested predominantly in ionized impurity scattering in the region $N > 10^{19}$ cm^{-3}.

Table 2: Fit parameters for μ=f(N) (Masetti's formula, equ. 3) for phosphorous- and boron-doped silicon [14] and zinc oxide, indium oxide and tin oxide
(μ_{max} - lattice mobility, μ_{min} - ionized impurity mobility, μ_{min} - μ_1 - clustering mobility)

Fit parameter	Si:P	Si:B	ZnO	ITO	SnO_2
μ_{max} [cm^2/Vs]	1414	470.5	210	210	250
μ_{min} [cm^2/Vs]	68.5	44.9	55	55	50
μ_{min} - μ_1 [cm^2/Vs]	12.4	15.9	5	5	10
n_{refl} [10^{17} cm^{-3}]	0.92	2.23	4	15	20
α_1	0.711	0.719	1	1	1
n_{ref2} [10^{20} cm^{-3}]	3.41	6.1	6	20	6
α_2	1.98	2.0	2	2	2

For the other two oxide materials mobility data of single crystals are even more rare. The few data points available have been added to Fig.1. For doped indium oxide single crystals also data of Kanai [16] were included (open triangles). However, these data seem to be too high compared to the other oxides and especially compared to silicon, having in mind that the universal process of ionized-impurity scattering is dominant in this range of carrier concentrations. Therefore, the data of Kanai were not used for fitting. Due to the lack of more data the single crystal mobilities of ITO and SnO_2 have been fitted with similar parameters as used for zinc oxide (see table 2).

Neutral impurity scattering. Neutral shallow-impurity scattering is often discussed in papers about transport in TCO films at room temperature [17,18]. The mobility due to neutral impurity scattering was first derived by Erginsoy [19] who scaled the electron scattering at hydrogen atoms to a semiconductor by using its dielectric constant and carrier effective mass, which leads to :

$$\mu_n = \frac{m^* e^3}{A(T) 4\pi\varepsilon\varepsilon_0 \hbar^3 N_n} \qquad (4).$$

Here, A(T) is the scattering cross-section factor and N_n is the density of neutral scattering centers. Erginsoy [19] calculated a temperature-independent value A=20, which is used mostly.

Itoh used the correct e-H scattering cross section to describe low-temperature electron and hole mobilities in germanium [20]. The concentration of neutral impurities is given by $N_n = N_D - N_A - n(T)$, where N_D and N_A are the donor and acceptor concentrations, respectively. Since the shallow donors in TCO materials (for instance the group III elements in ZnO) exhibit ionization energies around about 50 meV [21] the concentrations of neutral donors at

room temperature is very low, taking into account the further reduction of the ionization energy for degenerately doped semiconductors. Therefore, in this article this scattering process is not taken into consideration.

Dislocation scattering. Dislocation scattering seems to be a natural scattering process in polycrystalline materials. However, this process is rarely used in explaining experimental data of carrier transport in polycrystalline semiconductors and especially transparent conducting oxides [18]. Pödör [22] investigated bended Ge crystals with a dislocation density around 10^7 cm^{-2} and could his results desrcibe by equ. (5), taking into account scattering by charged dislocations (see also Seeger [23]):

$$\mu_{disl} = \frac{30\sqrt{2\pi}\left(\varepsilon_r \varepsilon_0\right)^{3/2} a^2 \sqrt{n}\, kT}{e^3 f^2 \sqrt{m^*} N_{disl}} \qquad (5),$$

where a is the distance between acceptor centers along the dislocation line, f is the occupation rate of these acceptors and N_{disl} is the density of dislocations.

Grain barrier limited transport. Polycrystalline films exhibit, depending on their mean grain size, a vast amount of grain barriers, which constitute crystallographically disturbed regions, leading to electronic defects in the band gap of semiconductors. These defects are charged by carriers from the grains. Charge balance causes a depletion zone on both sides of a grain barrier accompanied by an energetic barrier of height E_b for the carriers. The carrier transport in polycrystalline silicon was first described by Seto [24]. An improved model was presented by Baccarani et al. [25]. For our discussion it is sufficient to use Setos model. Both models yield an effective mobility μ_{eff} dominated by thermionic emission across the grain barriers with an energetic height E_b:

$$\mu_{eff} = \mu_0 \cdot \exp(-E_b/kT) \qquad (6)$$

where E_b is the energetic barrier height at the grain boundary, T the sample temperature, e and k are the elementary charge and the Boltzmann constant, respectively. Depending on the doping concentration in the grains, two expressions for the barrier height can be derived:

$$E_b = \frac{e^2 Q_t^2}{8\varepsilon\varepsilon_0 N} \qquad \text{for } LN > Q_t \qquad (7a),$$

$$E_b = \frac{e^2 L^2 N}{8\varepsilon\varepsilon_0} \qquad \text{for } LN < Q_t \qquad (7b),$$

where Q_t is the charge carrier trap density at the boundary, $\varepsilon\varepsilon_0$ is the static dielectric constant, N is the carrier density in the bulk of the grain and L the grain size. The prefactor μ_0 in (6) can be viewed as the mobility inside a grain given by [24]:

$$\mu_0 = \frac{e\,L}{\sqrt{2\pi m^* kT}} \qquad (7c).$$

For $LN > Q_t$ the traps are partially filled and hence the crystallites are completely depleted, while for $LN < Q_t$ only part of the grain is depleted and the traps are filled completely. The maximum barrier height E_{bmax} occurs for a doping concentration of $N(E_{bmax}) = Q_t/L$, accompanied by a minimum of the effective mobility according to equ. (6).
Recently, Lipperheide and Wille [26-28] worked out a theory for the combined ballistic and diffusive transport across grain barriers, which was applied to the carrier transport in polycrystalline silicon films [29,30]. However, their numerical approach yields only a marginal improvement compared to the analytical model of Seto.

3. Experimental details

The ZnO films were deposited by magnetron sputtering from a ceramic ZnO:Al2wt% target (76 mm diameter) in a home-made load-lock sputtering system with a base pressure of $5 \cdot 10^{-6}$ Pa. Radio frequency plasma excitation (13.56 and 27.12 MHz) with sputtering powers from 25 to 100 W was used for the film depositions. The samples were prepared at pressures in the range from 0.2 to 3.2 Pa; most of them at a total sputtering pressure of 0.4 Pa.
The substrates with a size of 10x10x0.5(1) mm^3 were radiatively heated by a boron nitride encapsulated graphite heater up to temperatures of 800 K. Both, amorphous float glass substrates as well as single crystalline substrates - silicon, sapphire (Al_2O_3) and periclase (MgO) - were used. The sapphire samples had different orientations: (001) or c-plane, (110) or a-plane and (012) or r-plane. Details on the structural characterization of these samples were presented recently [31].
The ITO films were deposited either by reactive magnetron sputtering from a metallic InSn10wt% target (76 mm diameter) or by sputtering in an pure Ar/O_2 atmosphere from a ceramic $In_2O_3SnO_2$10wt% target. These depositions have been performed in a commercial load-lock deposition system (LEYBOLD Z400) with a base pressure of about $3 \cdot 10^{-4}$ Pa. For

the reactively sputtered films the oxygen flow was varied from 6 to 8 sccm yielding conductive and opaque (low oxygen flows) films as well as transparent films with low and high resistivities (medium to high oxygen flows). In this way the electron concentration could be varied from about 10^{18} to 10^{21} cm^{-3}.

The film thickness was measured with a surface profiler (DEKTAK 3030) at a step in the film. The sheat resistances were measured by a 4-point probe. Conductivity and Hall measurements (magnetic flux of 0.86 T) were performed with the samples contacted in the van der Pauw geometry by room-temperature evaporation of Au/Ni (200/5 nm) contact triangles.

4. Results

A. Zinc oxide

Fig.2 shows our own mobility data for Al-doped ZnO films deposited both on glass and sapphire substrates as a function of the carrier concentration. The semiempirical fit curve from Fig.1 is also given together with experimental data of other groups: Minami et al. [2], Kon et al. [32] and Brehme et al. [33]. The mobility data of the single crystalline films are almost comparable to the literature data reported for ZnO films grown on glass substrates, though these films exhibit a significantly better crystalline quality compared to films grown on glass or silicon [31]. This means that for carrier concentrations above $1\text{-}3 \cdot 10^{20}$ cm^{-3} the mobility is dominated by ionized impurity scattering as already pointed out by Bellingham et al., Minami and Ellmer [1-3] (see also section 2). If the carrier concentration is reduced below about $3 \cdot 10^{20}$ cm^{-3} the mobility in the epitaxial films decreases steeply. This is in qualitative agreement with data of Minami [34] for undoped ZnO films and with data of Brehme et al. [33] and Kon et al. [35] for ZnO:Al films. The data of the latter two groups exhibit lower mobilities at all, perhaps caused by additional scattering centers due to crystallographic defects (see below). Comparable trends were also reported recently by Agashe et al. [36]; these data were not included in order not to overload Fig.2. Using equ.(6), the experimental data for $N < 3 \cdot 10^{20}$ cm^{-3} have been fitted (thin lines) for the data of Minami [34] for nominally undoped polycrystalline ZnO films and for the epitaxial ZnO:Al films. The following trap densities Q_t at the grain boundaries had to be assumed to fit the experimental data for ZnO and ZnO:Al films: $Q_{t(ZnO)} = 7 \cdot 10^{12}$ cm^{-2}; $Q_{t(ZnO:Al)} = 1.3 \cdot 10^{13}$ cm^{-2}. Also the other data have been fitted in order to determine the grain boundary trap densities which are summarized in table 3. It is interesting to note that the trap density changes significantly (by about a factor of 6) depending on the deposition conditions. The highest Q_t values occur for DC or pulsed-DC plasma excitation; RF magnetron sputtering reduces Q_t already by a factor

of 2.5. The lowest trap densities are achieved by magnetron sputtering onto substrates mounted perpendicularly relative to the sputtering target (Minami et al. [37], which reduces direct particle bombardment of the growing films), and for pulsed laser deposition [38,39]. This dependence points to the decisive role of the energy of the species contributing to the film growth, which will be discussed in section 6.

Table 3: Trap densities Q_t of zinc oxide and other polycrystalline films

Film:dopant	Growth	Method	Q_t [cm^{-2}]	Source
ZnO:Al	epitaxial	MS (RF)	$1.3 \cdot 10^{13}$	[31]
ZnO:Al	poly	RMS (DC)	$3 \cdot 10^{13}$	[33]
ZnO:Al	poly	RMS (MF)	$3 \cdot 10^{13}$	[35]
ZnO	poly	MS* (RF)	$7 \cdot 10^{12}$	[2]
ZnO:Al,Ga	epitaxial	PLD	$5 \cdot 10^{12}$	[39]
ZnO	epitaxial	PLD	$1.5 \cdot 10^{13}$	[40]
Si:P	poly	LPCVD/ MS	$3 - 3.8 \cdot 10^{12}$	[24,25]
Si:As,B,	poly	LPCVD	$3.6 \cdot 10^{12}$	[41]
CdS	poly	E	$1 \cdot 10^{12}$	[42]
FeS_2:Co	poly	MOCVD	$1.2 \cdot 10^{13}$	[43]

MS – magnetron sputtering, RMS – reactive magnetron sputtering, LPCVD- low pressure chemical vapour deposition, E – evaporation, MOCVD- metal organic chemical vapour deposition, PLD – pulsed laser deposition,
* substrates arranged perpendicularly relative to the sputtering target

The compilation of Table 3 shows, that grain barriers or other structural inhomogeneities affect significantly the carrier transport in polycrystalline as well as heteroepitaxially grown semiconducting films, independently of the material. For instance, also for gallium nitride films grown by MOCVD on sapphire substrates [44] and for GaAs layers [45] internal potential barriers (i.e. grain barriers) were recently reported to influence the carrier transport.
Annealing the ZnO:Al films in vacuum at about 500 °C caused a surprising result, depicted by the arrow in Fig.2. While the carrier concentration does not change at all, the mobility is increased by about 30 to 50%, approaching the mobility values of the general fit curve.
Even more important is the fact that this significant electrical improvement is not accompanied by a change of the structural parameters as measured by X-ray diffraction: strain, grain size, and orientation [31]. This means that no recrystallization has occured. Instead, it is plausible that the point defect and/or dislocation density has been reduced. Since the highest defect density exists at the grain boundaries [46], the annealing of the above mentioned defects most probably takes place also mainly at grain boundaries, thus reducing the grain barrier height leading to a higher mobility.
With this reasoning one can also explain that other mobility data from literature (see the data of [33,35] in Fig.2) have a comparable dependence on N as mentioned above, although their

absolute values are lower by a factor of 2 to 4. Probably, their samples, deposited under different deposition conditions, contain a higher amount of point defects and/or dislocations at grain boundaries, leading to higher grain barriers and lower mobilities.

Mobility data of films prepared by pulsed laser deposition, recently published by Lorenz et al. [39], are also included in Fig.2. Interestingly, these films exhibit mobilities that are comparable to mobility values reported for zinc oxide single crystals, pointing to a higher structural quality and hence a lower grain barrier defect density of these PLD films. However, a tendency to lower mobilities (compared to single crystal values) can also be observed for $N < 1 \cdot 10^{19}$ cm^{-3} which can be explained by a trap density of $Q_{t(PLD)} = 5 \cdot 10^{12}$ cm^{-2}.

A further confirmation of the decisive role of grain barriers comes from data published recently by Makino et al. [40]. These authors deposited ZnO films by pulsed laser ablation at 600 °C onto lattice-matched $ScAlMgO_4$ (SCAM) substrates. Though the films exhibit a very high structural quality, due to the small lattice mismatch, their carrier concentration-dependent mobilities exhibit a "mobility hole" (see Fig.3), which was not be explained by the authors. Only at low and high carrier concentrations the film mobilities fit to the semiempirical mobility fitting curve for ZnO (Fig.1, 2). However, the dramatic decrease of μ around a carrier concentration of $N \approx 2 \cdot 10^{19}$ cm^{-3}, which resembles the corresponding μ-dependence of polycrystalline silicon of Seto [24], can be explained by grain barrier scattering, if one assumes a trap density of $Q_{t(PLD\text{-}Makino)} = 1.5 \cdot 10^{13}$ cm^{-2}. What is not clear in this explanation is the high defect density compared to the PLD-layers of Lorenz et al.; perhaps Makino et al. used higher plasma densities at the growing films leading to higher defect densities.

It has to be mentioned, that the experimental dependence $\mu = f(N)$ for $N > 5 \cdot 10^{20}$ cm^{-3} can only be explained by taking into account the effect of impurity clustering (see [11-13]) and nonparabolicity of the conduction band of ZnO which was shown already recently [3].

B. Indium tin oxide

The ITO mobility data versus the carrier concentration are displayed in Fig.4. Our own measurements for films deposited at different conditions with respect to substrate temperature, target material and plasma excitation frequency are compared with data from literature. The carrier concentration in the films was varied by changing the oxygen partial pressure. It is interesting to note that opaque films (displayed by filled symbols), deposited at low oxygen flows, exhibit quite low mobilities. Possibly, these low mobilities, despite a high carrier concentration, are caused by a percolation of the electron paths in a heterogeneous mixture of oxide and metal clusters, i.e. the cermet-like structure of these opaque films [47].

The highest carrier concentrations of about $1 \cdot 10^{21}$ cm^{-3} occur at the transition from opaque to transparent films, accompanied by a step-like increase of the mobility values from about 20 to 30 cm^2/Vs. Further increasing the oxygen partial pressure leads to a decrease of the carrier density and a slight increase of the mobility to values around 40 cm^2/Vs, which stay constant down to carrier concentrations of about 10^{18} cm^{-3}. This behaviour is significantly different compared to zinc oxide, obviously due to different grain barrier trap densities of ZnO and ITO. At a carrier concentration below about 10^{18} cm^{-3} a decrease of the mobility can be seen, which we interpret as the onset of grain barrier limited transport. Fitting the experimental data by the expression (6,7) leads to a grain barrier trap density of $1.5 \cdot 10^{12}$ cm^{-2}, much lower than that of the magnetron sputtered ZnO:Al films. On the other hand, the mobility data of Szczyrbowski et al. [48], also shown in Fig.3, exhibit a behaviour similar to the ZnO:Al films. Only for very high carrier concentrations the mobility is in the range of 40 – 50 cm^2/Vs, comparable to our own ITO films. With decreasing N the mobility decreases strongly, which points to a much higher trap density of $Q_t = 2.5 \cdot 10^{13}$ cm^{-2}. This high Q_t value becomes plausible, taking into account the deposition method used by Szczyrbowski et al.: reactive diode sputtering with discharge voltages around 2000 V, which is much higher than typical target voltages for magnetron sputtering (< 500 V). This means energetic bombardment during film growth introduces a high defect density, even at a substrate temperature of 400 °C, used by Szczyrbowski et al., where the damage can be annealed out at least partially. We have also found (not shown), that the μ(N)-dependence for undoped indium oxide (In_2O_{3-x}) is comparable to that of ITO. Therefore, the dopant tin seems to be not responsible for this electrical transport property of indium oxide.

6. Discussion

Obviously, the charge trap densities of TCO films prepared by different methods vary significantly, covering the range of $1.5 \cdot 10^{12}$ to $3 \cdot 10^{13}$ cm^{-2}. These values are in the upper region compared to polycrystalline silicon or gallium arsenide, which is plausible taking into account that the TCO films were prepared with ion-assistance. Furthermore, in polycrystalline silicon the trap density can be reduced significantly by annealing or deposition in hydrogen-containing atmospheres, which is not really viable for oxides due to the reducing effect of hydrogen.

From table 4 one can infere that the defect density is correlated with the discharge modus, especially with the discharge voltage. This means, the energy of the particles contributing to or assisting the film growth significantly influences the defect density. This can be seen both

for ZnO as well as for ITO. However, for comparable deposition conditions in ZnO the defect density is higher than that of ITO, which seems to be caused by a lower defect formation energy in ZnO and/or self-annealing effects in ITO.

Since ionized-impurity scattering is a universal process for homogeneously doped semiconductors and since the material parameters (ε_r and m*, see equ. 1) are comparable for the TCO materials, the clear differences between the TCOs should be caused by other reasons, which can not be inferred directly from our integral transport measurements. In the

Table 4: Trap densities Q_t of epitaxial and polycrystalline TCO films

Film:dopant	Growth	Method	Excitation (U_{dis} [V])	Q_t [cm^{-2}]	Source
ZnO:Al	epitaxial	MS	RF (200)	$1.3 \cdot 10^{13}$	[31]
ZnO:Al	on glass	RMS	DC (425)	$3 \cdot 10^{13}$	[33]
ZnO:Al	on glass	RMS	MF (340)	$3 \cdot 10^{13}$	[35]
ZnO	on glass	MS*	RF	$7 \cdot 10^{12}$	[2]
ZnO:Al,Ga	epitaxial	PLD	-	$5 \cdot 10^{12}$	[39]
ZnO	epitaxial	PLD	-	$1.5 \cdot 10^{13}$	[40]
In_2O_3:Sn	on glass	RMS/MS	DC (400) RF (250)	$1.5 \cdot 10^{12}$	this work
In_2O_3:Sn	on glass	MS	RF-diode (2000)	$2.5 \cdot 10^{13}$	[48]
SnO_2:F,Cl	on glass	SP	-	$4 \cdot 10^{12}$	[49]
$CdIn_2O_4$	on glass	RMS	DC (2000)	$1.5 \cdot 10^{13}$	[6]

RMS, MS – reactive magnetron sputtering, PLD – pulsed laser deposition, SP – spray pyrolysis, DC, RF, MF – direct current, radio frequency, mid frequency excitation, p-DC – pulsed DC excitation, * - substrates arranged perpendicular to the target (reduced ion bombardment)

following some possible reasons are discussed, based on a literature survey and on calculations. An interesting explanation of a strongly reduced mobility in heavily doped n-type GaAs ($n > 3 \cdot 10^{18}$ cm^{-3}) was given by Walukiewicz [50]. He assumes the formation of compensating native defects (gallium vacancies V_{Ga} for n-GaAs) which act as scattering centers. With this model Walukiewicz can explain the mobility in n-GaAs. Crucial in his model is the defect formation energy for V_{Ga}, which depends on the position of the Fermi level. Such a mechanism could also effect the mobility in TCO materials.

In the following possible reasons for different defect formation energies in ZnO and ITO are discussed:

ZnO. Recently, heteroepitaxial ZnO films grown on GaN films on sapphire substrates were analyzed by transmission electron microscopy [51]. These films are characterized by a high stacking fault density in the range of 10^{18} cm^{-3}. According to Gerthsen et al. [51] these

stacking faults are mainly generated by the precipitation of Zn interstitials accompanied by the formation of oxygen vacancies in the vicinity of a stacking fault. Since oxygen vacancies exhibit a charge of Z = 2 its scattering power is higher than that of singly ionized dopands like the group III elements in ZnO (B^+, Al^+, Ga^+, Z=1) leading to a reduced mobility.

For polycrystalline films an even higher stacking fault and dislocation density is plausible. Sagalowicz and Fox [52] analyzed undoped polycrystalline ZnO films by TEM and found dislocation densities of around 10^{12} cm^{-2}, corresponding to a mean distance of 10 nm. Hence, the scattering of carriers at dislocations and oxygen vacancies would be even higher in such materials. Recent density-functional calculations [53] have shown that „point defect formation enthalpies in zinc oxide are very small“ supporting the considerations given above. It is also noteworthy that ZnO exhibits a high radiation hardness, which is likely due to a rapid annealing of Frenkel pairs [54,55], again caused by low defect formation energies, leading to high diffusion coefficients. Zinc oxide is a polar semiconductor, i.e. electrical charges are induced by stress along the c-axis. Its piezoelectric properties are the reason for its use in surface acoustic wave (SAW) devices [56]. With this respect ZnO is similar to GaN [57]. This means intrinsic stress, due to lattice mismatch and/or to growth defects could induce charges at grain barriers or extended defects leading to additional scattering.

ITO. In contrast to ZnO and GaN, indium oxide is a cubic material which exhibits no piezoelectric effect. Therefore, the number of charged defects should be significantly lower in ITO. Indium oxide is also peculiar in this respect, that even amorphous ITO films exhibit quite high mobilities [58,59], which contrasts with the common wisdom of semiconductor physicists that the mobility is highest in semiconductors of high structural quality.

A recent X-ray photoelectron spectroscopy study [60] of magnetron sputtered ITO films showed that the surface of highly conducting ITO is metallic, which is not caused by conduction band electrons but by metallic surface states. The same situation could apply also at grain barriers, which would explain low barrier heights and thus high mobilities even at low carrier concentrations.

On the other hand, indium oxide is also prone to defect formation by energetic species during the deposition process, which can be inferred from Fig.3. For instance, Utsumi et al. [61] reported that even a reduction of the discharge voltage from 280 to 260 V decreased the resistivity by an increased mobility. However, for deposition processes like magnetron sputtering, with moderate particle energies, the defect formation seems to be comparably low.

7. Conclusions

By comparing the mobility-dependences as a function of the carrier concentration for systematic series of indium oxide and zinc oxide films it was elucidated that the grain barrier trap densities of ITO and ZnO are significantly different, covering the range of $1.5 \cdot 10^{12}$ to $3 \cdot 10^{13}$ cm^{-2}. Also for the same oxide different trap densities were found that could be correlated with the deposition method, especially with the discharge voltage during magnetron sputtering: higher particle energies in the deposition process lead to higher trap densities. These differences can not be explained by ionized impurity scattering, the process mostly used for the explanation of the mobilities for carrier concentrations above 10^{20} cm^{-3}. Taking into account the defect chemistry and the formation of planar defects in these oxides plausible reasons are given for the observed grain barrier densities. Especially remarkable is the piezoelectricity of ZnO along the c-axis, which distinguishes the polar ZnO from the cubic In_2O_3 lattice.

One strategy to reduce the resistivity of zinc oxide further could be to find deposition processes or to use crystalline substrates which lead to ZnO films without a preferred texture along the polar c-axis.

7. References

[1] J. R. Bellingham, W. A. Phillips and C. J. Adkins, J. Mat. Sci. Lett. 11 (1992) 263.
[2] T. Minami, MRS Bull. 25 (2000) 38.
[3] K. Ellmer, J. Phys. D: Appl. Phys. 34 (2001) 3097.
[4] W. Shockley, "Electrons and Holes in Semiconductors" (van Nostrand, Toronto, 1950).
[5] R. B. Dingle, Phil. Mag. 46 (1955) 831.
[6] T. Pisarkiewicz, K. Zakrzewska and E. Leja, Thin Solid Films 174 (1989) 217.
[7] W. Zawadzki, in "Handbook on Semiconductors", Ed.: T. S. Moss (North-Holland, Amsterdam, 1982), p. 713.
[8] E. Conwell and V. F. Weisskopf, Phys. Rev. 77 (1950) 388.
[9] E. Conwell and V. F. Weisskopf, Phys. Rev. 69 (1946) 258.
[10] I. V. Dakhovskii, T. A. Polyanskaya, A. G. Samoilovich and Y. V. Shartsev, Soviet Phys.-Semicond. 4 (1971) 1857.
[11] D. B. M. Klaassen, Solid-State Electr. 35 (1992) 961.
[12] D. B. M. Klaassen, Solid-State Electr. 35 (1992) 953.
[13] P. Ebert, Z. Zhang, F. Kluge, M. Simon, Z. Zhang and K. Urban, Phys. Rev. Lett. 83 (1999) 757.
[14] G. Masetti, M. Severi and S. Solmi, IEEE Trans. Electron Dev. ED30 (1983) 764.
[15] H. Rupprecht, J. Phys. Chem. Solids 6 (1958) 144.
[16] Y. Kanai, Jap. J. Appl. Phys. 23 (1984) 127.
[17] D. Mergel and Z. Qiao, J. Appl. Phys. 95 (2004) 5608.
[18] H. L. Hartnagel, A. L. Dawar, A. K. Jain and C. Jagadish, "Semiconducting Transparent Thin Films" (Institute of Physics Publishing, Bristol, 1995).
[19] C. Erginsoy, Phys. Rev. 79 (1950) 1013.
[20] K. M. Itoh, W. Walukiewicz, H. D. Fuchs, J. W. Beeman, E. E. Haller, J. W. Farmer and V. I. Ozhogin, Phys. Rev. B 50 (1994) 16995.
[21] B. K. Meyer, J. Sann, D. M. Hofmann, C. Neumann and A. Zeuner, Semicond. Sci. Techn. 20 (2005) S62.
[22] B. Pödör, phys. stat. sol. 16 (1966) K167.
[23] K. Seeger, "Semiconductor Physics" (Springer, Berlin, 1991).

[24] J. Y. Seto, J. Appl. Phys. 46 (1975) 5247.
[25] G. Baccarani, B. Ricco and G. Spadini, J. Appl. Phys. 49 (1978) 5565.
[26] R. Lipperheide, T. Weis and U. Wille, Solar Energy Mat. Solar Cells 65 (2001) 157.
[27] R. Lipperheide, T. Weis and U. Wille, J. Phys.: Condens. Matter 13 (2001) 3347.
[28] R. Lipperheide and U. Wille, Phys. Rev. B 68 (2003) 115315.
[29] T. Weis, S. Brehme, P. Kanschat, W. Fuhs, R. Lipperheide and U. Wille, J. Non-Cryst. Solids 299–302 (2002) 380–384.
[30] T. Weis, R. Lipperheide, U. Wille and S. Brehme, J. Appl. Phys. 92 (2002) 1411.
[31] K. Ellmer and G. Vollweiler, Thin Solid Films 496 (2006) 104.
[32] M. Kon, P. K. Song, Y. Shigesato, P. Frach, A. Mizukami and K. Suzuki, Jap. J. Appl. Phys. 41 (2002) 814.
[33] S. Brehme, F. Fenske, W. Fuhs, E. Neubauer, M. Poschenrieder, B. Selle and I. Sieber, Thin Solid Films 342 (1999) 167.
[34] T. Minami, S. Suzuki and T. Miyata, Mat. Res. Soc. Symp. Proc. 666 (2001) F1.3.1.
[35] M. Kon, P. K. Song, Y. Shigesato, P. Frach, S. Ohno and K. Suzuki, Jap. J. Appl. Phys. 42 (2003) 263.
[36] C. Agashe, O. Kluth, J. Hüpkes, U. Zastrow, B. Rech and M. Wuttig, J. Appl. Phys. 95 (2004) 1911.
[37] H. Nanto, T. Minami, S. Shooji and S. Takata, J. Appl. Phys. 55 (1984) 1029.
[38] A. Suzuki, T. Matsushita, N. Wada, Y. Sakamoto and M. Okuda, Jap. J. Appl. Phys. 35 (1996) L56.
[39] M. Lorenz, E. M. Kaidashev, H. von Wenckstern, V. Riede, C. Bundesmann, D. Spemann, G. Benndorf, H. Hochmuth, A. Rahm, H.-C. Semmelhack and M. Grundmann, Solid-State Electr. 47 (2003) 2205.
[40] T. Makino, Y. Segawa, A. Tsukazaki, A. Ohtomo and M. Kawasaki, Appl. Phys. Lett. 87 (2005) 022101.
[41] J. Werner and M. Peisl, Phys. Rev. B 31 (1985) 6881.
[42] L. L. Kazmerski, W. B. Berry and C. W. Allen, J. Appl. Phys. 43 (1972) 3515.
[43] J. Oertel, K. Ellmer, W. Bohne, J. Röhrich and H. Tributsch, J. Crystal Growth 198/199 (1999) 1205.
[44] H. Witte, A. Krtschil, E. Schrenk, K. Fluegge, A. Dadgar and A. Krost, J. Appl. Phys. 97 (2005) 043710.
[45] V. Kazukauskas, G. Kühnel and W. Siegel, Appl. Phys. Lett. 70 (1997) 1751.
[46] F. M. Hossain, J. Nishi, S. Takagi, A. Ohtomo, T. Fukumura, H. Fuijioka, H. Ohno, H. Koinuma and M. Kawasaki, J. Appl. Phys. 94 (2003) 7768.
[47] J. Ederth, G. A. Niklasson, A. Hultaker, P. Heszler, C. G. Granqvist, A. R. van Doorn, M. J. Jongerius and B. Burgard, J. Appl. Phys. 93 (2003) 984.
[48] J. Szczyrbowski, K. Schmalzbauer and H. Hoffmann, Thin Solid Films 137 (1986) 169.
[49] A. Messad, J. Bruneaux, H. Cachet and M. Froment, J. Mat. Sci. 29 (1994) 5095.
[50] W. Walukiewicz, Phys. Rev. B 41 (1990) 10218.
[51] D. Gerthsen, D. Litvinov, T. Gruber, C. Kirchner and A. Waag, Appl. Phys. Lett. 81 (2002) 3972.
[52] L. Sagalowicz and G. R. Fox, J. Mater. Res. 14 (1999) 1876.
[53] P. Erhart, K. Albe and A. Klein, Phys. Rev. B 73 (2006) 205203.
[54] P. Erhart and K. Albe, Appl. Phys. Lett. 88 (2006) 201918.
[55] C. Coskun, D. C. Look, G. C. Farlow and J. R. Sizelove, Semicond. Sci. Techn. 19 (2004) 752.
[56] N. W. Emanetoglu, C. Gorla, Y. Liu, S. Liang and Y. Lu, Mat. Sci. Semicond. Proc. 2 (1999) 247.
[57] J. J. Harris, K. J. Lee, J. B. Webb, H. Tang, I. Harrison, L. B. Flannery, T. S. Cheng and C. T. Foxon, Semicond. Sci. Techn. 15 (2000) 413.
[58] J. R. Bellingham, W. A. Phillips and C. J. Adkins, J. Phys.: Condens. Matt. 2 (1990) 6207.
[59] M. P. Taylor, D. W. Readey, C. W. Teplin, M. F. A. M. van Hest, J. L. Alleman, M. S. Dabney, L. M. Gedvilas, B. M. Keyes, B. To, J. D. Perkins and D. S. Ginley, Meas. Sci. Techn. 16 (2005) 90.
[60] Y. Gassenbauer and A. Klein, J. Phys. Chem. B 110 (2006) 4793.
[61] K. Utsumi, O. Matsunaga and T. Takahata, Thin Solid Films 334 (1998) 30.
[62] A. R. Hutson, Phys. Rev. 108 (1957) 222.
[63] D. G. Thomas and J. J. Lander, in "Halbleiter und Phosphore", Ed.: M. Schön and H. Welker (Vieweg, Braunschweig, 1958), p. 534.
[64] W. S. Baer, Phys. Rev. 154 (1967) 785.
[65] A. Hausmann and W. Teuerle, Z. Phys. 259 (1973) 189.
[66] P. Wagner and R. Helbig, J. Phys. Chem. Solids 35 (1974) 327.
[67] B. Utsch and A. Hausmann, Z. Physik B 21 (1975) 27.
[68] K. I. Hagemark and L. C. Chacka, J. Solid State Chem. 15 (1975) 261.
[69] D. C. Look, D. C. Reynolds, J. R. Sizelove, R. L. Jones, C. W. Litton, G. Cantwell and W. C. Harsch, Solid State Comm. 105 (1998) 399.
[70] H. von Wenckstern, S. Weinhold, G. Biehne, R. Pickenhain, H. Schmidt, H. Hochmuth and M. Grundmann, Adv. Solid State Phys. 45 (2005) 263.
[71] Z. M. Jarzebski and J. P. Marton, J. Electrochem. Soc. 123 (1976) 299C.

[72] R. L. Weiher, J. Appl. Phys. 33 (1962) 2834.
[73] T. Minami, H. Sato, K. Ohashi, T. Tomofuji and S. Takata, J. Crystal Growth 117 (1992) 370.
[74] I. Hamberg and C. G. Granqvist, J. Appl. Phys. 60 (1986) R123.
[75] G. Frank and H. Köstlin, Appl. Phys. A 27 (1982) 197.
[76] H. Ohta, M. Orita, M. Hirano, H. Tanji, H. Kawazoe and H. Hosono, Appl. Phys. Lett. 76 (2000) 2740.

Figure captions

Fig.1: Hall mobility data, reported in literature, of undoped and doped zinc oxide single crystals as a function of the carrier concentration (squared and round symbols) [15,62-70]. A part of these data were already presented in [3]. Mobility values, shown as triangles, were reported for SnO_2 (▲) [71] and In_2O_3 (▼, ∇) [16,72] single crystals. The dotted and dashed lines show the mobility data of boron-doped and phosphorous-doped silicon [14] (equ.3 and table 2). The ZnO, ITO and SnO_2 data were also fitted by equ. (3), shown as solid lines, with parameters given in table 2.

Fig.2: Hall mobilities of undoped and doped zinc oxide thin films as a function of the carrier concentration. Our own data are shown for films deposited onto float glass (■) as well as sapphire substrates (Δ, ▷,◁,) [31]. For comparison mobility data of other groups were added, which have been measured for films deposited by magnetron sputtering and by pulsed laser deposition (PLD): Minami (□, #, ● - PLD) [73], Brehme et al. (▼, ∇) [33], Kon et al. (⊠) [35], Suzuki (○ - PLD) [38] and Lorenz et al. (⊗, ⊕ - PLD) [39]. The mobility values of ZnO single crystals (◆), already shown in Fig. 1 and the fit curve according to equ.(3), are also displayed. The thin film mobility data have been fitted by the combined ionized and grain boundary model (equ. 6, 7), yielding the grain boundary trap densities summarized in tables 3 and 4.

Fig.3: Hall mobility data of Makino et al. [40] for heteroepitaxial ZnO films deposited by pulsed laser deposition at 600 °C onto lattice-matched $ScAlMgO_3$ (SCAM) substrates. While the authors fit their data by the dashed theoretical curve taking into account different scattering mechanisms in ZnO (acustic, piezoelectric, polar-optical and ionized impurity scattering), the solid line is the semiempirical fit curve to the mobility data of single- and polycrystalline ZnO (Fig.1), which obviously better describes the general trend. The "mobility hole" around $N \approx 2 \cdot 10^{19}$ cm^{-3}, which was not explained by Makino et al., is fitted (dotted line) by the process of grain barrier-limited transport.

Fig.4: Hall mobility data of tin-doped indium oxide thin films as a function of the carrier concentration. Our own data are shown by open and filled symbols, while literature data are displayed by crosses (+ - diode sputtering [48], x - electron beam evaporation [74], # - spray pyrolysis [75]). Heteroepitaxial ITO films, grown by PLD were also included [76]. Two data sets have been fitted taking into account both ionized impurity and cluster scattering as well as grain barrier limited transport, shown as continuous and dashed lines.

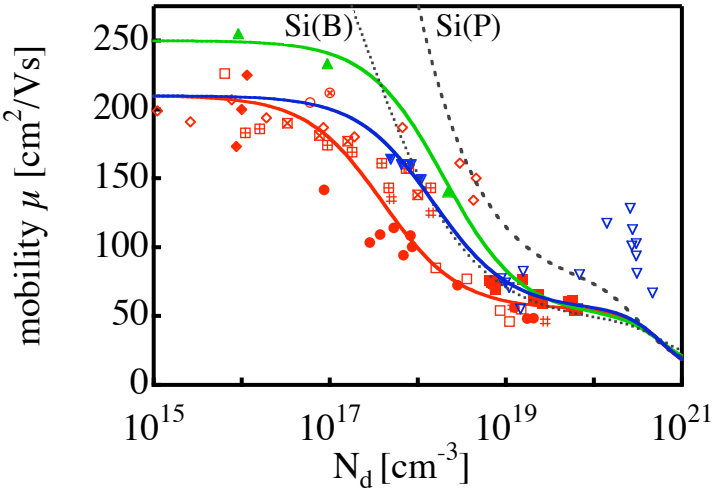
Si(B)
Si(P)
250
200
150
100
50
0
mobility μ [cm^2/Vs]
10^{15}
10^{17}
10^{19}
10^{21}
N_d [cm^{-3}]

Fig. 1

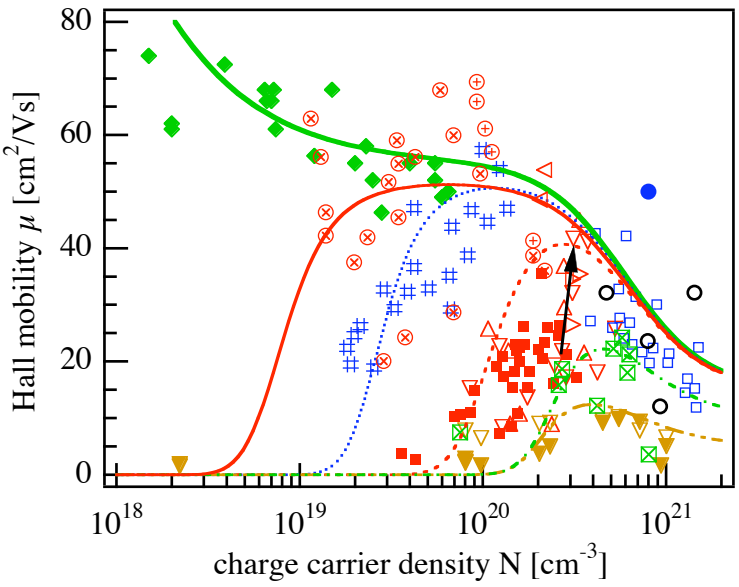
80
60
40
20
0
Hall mobility μ [cm²/Vs]
10¹⁸
10¹⁹
10²⁰
10²¹
charge carrier density N [cm⁻³]

Fig. 2

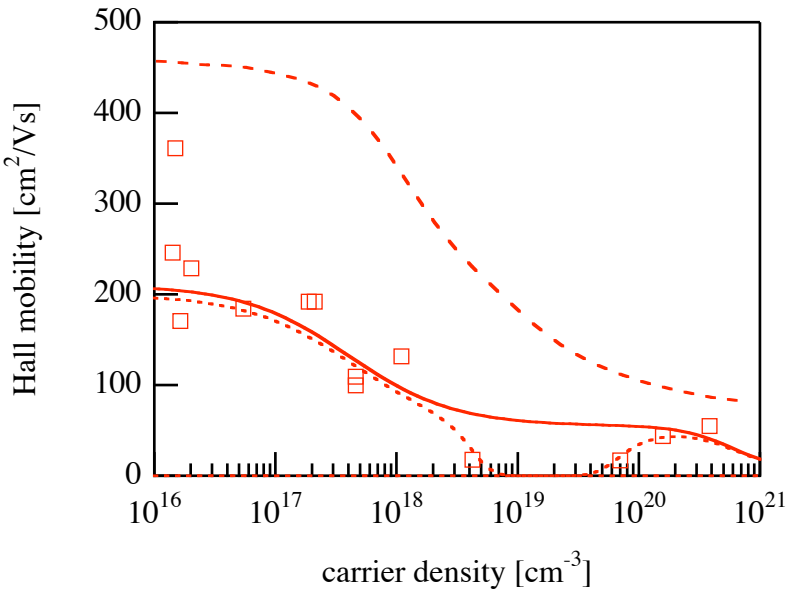
500
400
300
200
100
0
Hall mobility [cm^2/Vs]
10^{16}
10^{17}
10^{18}
10^{19}
10^{20}
10^{21}
carrier density [cm^{-3}]

Fig. 3

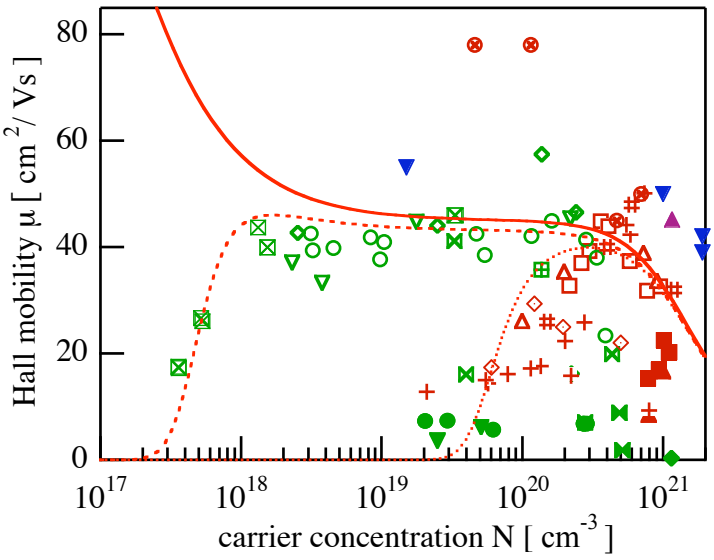
Hall mobility μ [cm 2 / Vs]
80
60
40
20
0
10^17
10^18
10^19
10^20
10^21
carrier concentration N [cm^-3]

Fig. 4